Electrochemically Modified Poly(dicyandiamide) Electrodes for Detecting Hydrazine in Neutral pH

Manavalan, Gopinathan; Natarajan, Thiyagarajan; Adeniyi, Kayode Omotayo; Zen, Jyh Myng; Tesfalidet, Solomon; Thyrel, Mikael; Lestander, Torbjörn A.; Alla, Subba Reddy; Mikkola, Jyri Pekka

Published in:
Industrial and Engineering Chemistry Research

DOI:
10.1021/acs.iecr.3c02669

Published: 08/11/2023

Document Version
Final published version

Document License
CC BY

I&EC research
Industrial & Engineering Chemistry Research

pubs.acs.org/IECR
Article

Electrochemically Modified Poly(dicyandiamide) Electrodes for Detecting Hydrazine in Neutral pH

Published as part of the Industrial & Engineering Chemistry Research virtual special issue "Dmitry Murzin Festschrift".

Gopinathan Manavalan,* Thiyagarajan Natarajan, Kayode Omotayo Adeniyi, Jyh-Myng Zen, Solomon Tesfalidet, Mikael Thyrel, Torbjörn A. Lestander, Subba Reddy Alla, and Jyri-Pekka Mikkola

Cite This: *Ind. Eng. Chem. Res.* 2023, 62, 18271−18279

Read Online

ACCESS | Metrics & More | Article Recommendations

ABSTRACT: A new technique for sensing nanomolar concentrations of hydrazine in water samples is reported. A screen-printed carbon electrode (SPCE) altered using an amine-azo functional group encompassing poly(dicyandiamide) is used in this study. The modified electrode exhibits an enhanced activity toward hydrazine detection at a lower overpotential and broad linear scale between 20 nM and 1 mM, with an accurate sensitivity value of 0.1 nA μm^{-1} cm^{-2}. To the best of our knowledge, poly(dicyandiamide)-modified electrodes exhibit one of the lowest limits of detection for any metal-free electrode that detects 6.7 nM (S/N = 3) of hydrazine. The method established sufficient selectivity and better recoveries. Finally, the poly(dicyandiamide)-modified SPCE* is highly suitable for electrochemical determination of hydrazine in water samples from tap and lake.

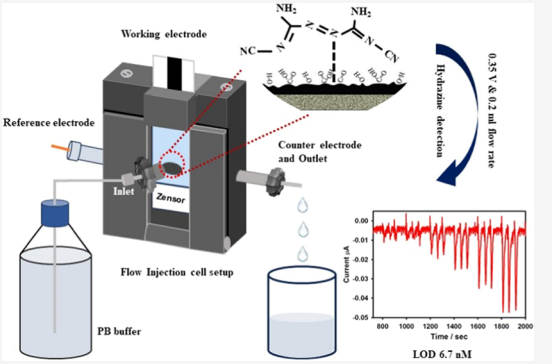

INTRODUCTION

Hydrazine, an intense reducing agent as well as a very reactive base, is often used for therapeutic purposes and in photography, pesticides, plant growth regulators, fuel cells, and textile industries. It is also prevalently utilized as a propellant in missile systems, a chemical blowing agent, an emulsifier, a corrosion inhibitor for heating systems, and an oxygen scavenger.[1−7] A prolonged exposure to moderate hydrazine levels can cause adverse health hazards to kidney and liver, weakening of the central nervous system (CNS) as well as brain, and DNA damage, whereas short-time contact can result in giddiness and irritation in the eyes, nose, and also in throat.[5,8,9] Owing to its toxic nature, hydrazine is categorized as a group-B2 human carcinogen.[4,10] Thus, it is essential to establish a precise technique to identify trace levels of hydrazine in both environmental and industrial samples.

There have been multiple detection methods reported for hydrazine determination, such as fluorimetry,[11] spectrophotometry,[12] chromatography techniques,[13,14] chemiluminescence,[15] surface-enhanced Raman spectroscopy,[16] and electrochemical sensors.[17,18] Although the electrochemical sensor method offers one of the simplest and cost-effective approaches with on-field sensing capability, hydrazine oxidation at the bare electrode is poorly catalyzed and requires a high overpotential.[19] Thus, several metal/metal oxide,[20−23] metal complex,[24] and organic mediator[19,25,26]-modified electrodes were developed. The chemically modified electrodes (CMEs) exhibit improved electron-transfer rate, catalytic activity, and lower detection overpotential[27−30] and are continuing to evolve.

Modifiers such as pyrocatechol violet, poly(vinylpyrrolidone), and poly(3,4-ethylenedioxythiophene):poly(styrene sulfonate) (PEDOT:PSS) were utilized for the determination of hydrazine.[19,31,32] Multilayer graphene nanobelts (GNBs) for hydrazine sensors are also being explored.[10] Similarly, glassy carbon electrodes modified with gold nanoparticle-decorated mesoporous silica microspheres (GC/Au-MSM),[7] growing hydroxyapatite *in situ* in a chemically reduced graphene oxide composite (HAP-rGO),[18] ZIF-8 on porous nickel films (ZIF-Ni),[33] and glassy carbon electrodes enhanced with cobalt oxide nanocubes combined with reduced graphene oxide on gold nanocomposite[34] are also reported. Despite larger specific surface area as well as

Received: July 31, 2023
Revised: October 11, 2023
Accepted: October 12, 2023
Published: October 25, 2023

https://doi.org/10.1021/acs.iecr.3c02669
Ind. Eng. Chem. Res. 2023, 62, 18271−18279

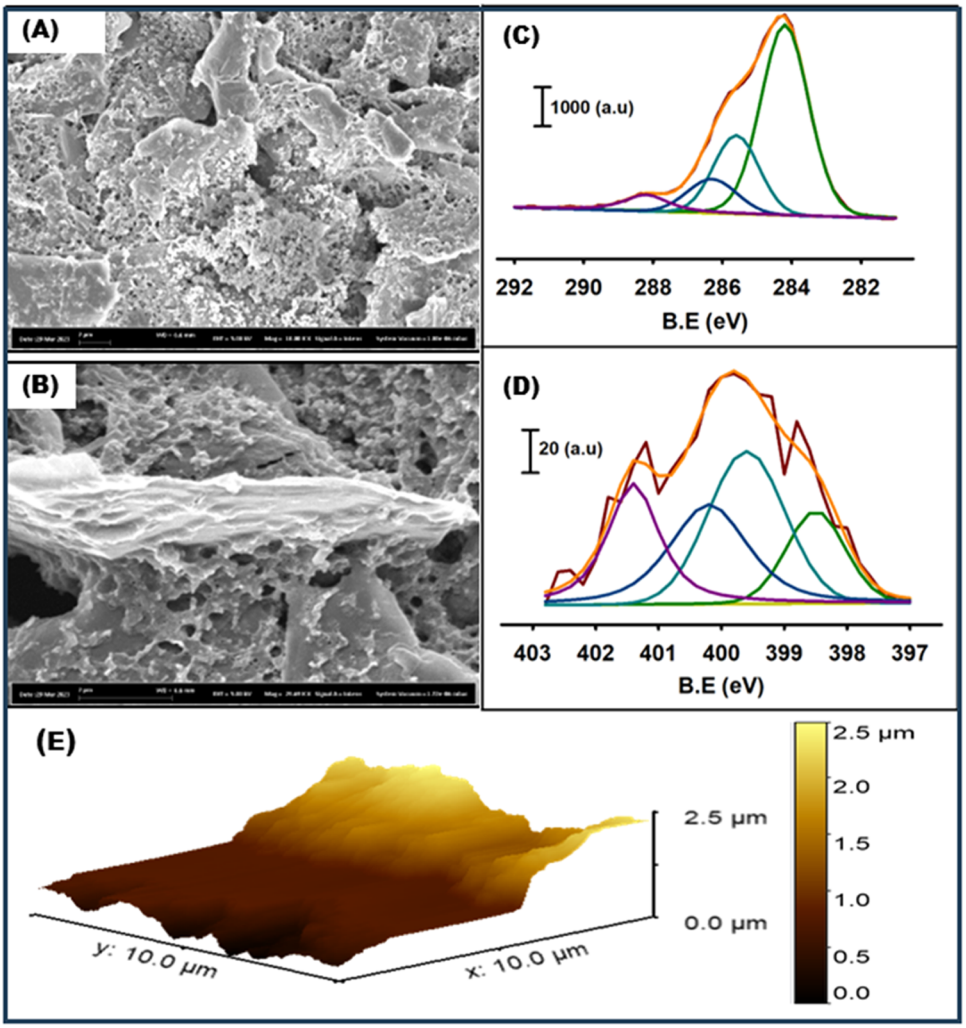

Figure 1. SEM images of the SPCE* (A) and DCD-SPCE* (B) (scale bar: 2 μm). Resolved C 1s of SPCE* (C) and resolved N 1s XPS spectra of DCD-SPCEs* (D). AFM image of the DCD-SPCE* (E).

improved conductivity, some of the systems suffer from long electrode preparation/renovation time, lower sensitivity, and complicated electrode preparation procedures.[35] Therefore, developing sensor systems that are cost-effective with good sensitivity is essential for large-scale applications. Along this line, a robust chemically modified electrode with superior sensitivity and tremendous catalytic activity toward hydrazine detection was evaluated.

In this study, we employed electrogenerated chlorine with a chloride-containing supporting electrolyte to introduce an amine-azo functional group encompassing poly-(dicyandiamide) onto a screen-printed carbon electrode (SPCE). This is the first report of in situ electrochemical synthesis of poly(dicyandiamide) on SPCEs*, resulting in the production of DCD-SPCE* specifically for the purpose of hydrazine detection. The poly(dicyandiamide)-modified SPCEs* are utilized to detect a minute amount of hydrazine in water samples. DCD-SPCE* exhibits an enhanced activity in the detection of hydrazine at a lower overpotential showing a specific sensitivity value of 0.1 nA μm^{-1} cm^{-2}. To the best of our knowledge, poly(dicyandiamide) electrodes exhibit one of the lowest limits of detection for any metal-free electrode showing a detection limit value of 6.7 nM.

EXPERIMENTAL SECTION

Chemicals and Reagents. 0.1 M Phosphate buffer solution (0.1 M) was produced by mixing 0.1 M Na_2HPO_4 (99.0%, Merck, Germany) with 0.1 M $NaH_2PO_4{\cdot}H_2O$ (98.0%, Merck, Germany) and then adjusted to a pH of 7.4 (0.1 M PB). Dicyandiamide was bought from Alfa Aesar, UK (DCD, $C_2H_4N_4$, 99%). Hydrazine was purchased from Sigma-Aldrich (HYZ, N_2H_4, 35%). We utilized analytical grade chemicals for this research, and Milli-Q distilled water from Millipore was employed to prepare aqueous solutions. No extra purification steps were carried out for any of the chemicals used.

Instrumentation and Software. We performed electrochemical experiments using either a CHI-832 electrochemical analyzer from CH Instruments or a Modulab potentiostat from Solartron Analytical, the United Kingdom. These experiments were conducted in a three-electrode cell. We employed a Zeiss Merlin FEG-SEM instrument to conduct scanning electron microscopy (SEM) in this study (Oberkochen, BW, Germany). X-ray photoelectron spectroscopy (XPS) characterizations were accomplished using an OmicronDAR 400. Atomic force microscopy (AFM) is performed in tapping mode with RTESP cantilevers using scan lines of 256 × 256 and a scan speed of 1 Hz (Multimode, Nanoscope IV controller, Bruker).

https://doi.org/10.1021/acs.iecr.3c02669
Ind. Eng. Chem. Res. 2023, 62, 18271−18279

Electrode Preparation. The disposable SPCE (electrode surface area = 0.196 cm^2) was sourced from Zensor R&D (Taiwan). In these studies, the SPCE underwent electrochemical cleaning through cyclic voltammetry technique ranging from −1.0 to 1.2 V versus Ag/AgCl in 0.1 M PB solution (6 segments). Subsequently, the SPCE was preanodized at 2.0 V, 5 min in 0.1 M PB solution (labeled as SPCE*). Further, the dicyandiamide was polymerized on the SPCE* through a potential cycling procedure spanning +0.2 to +1.55 V in a solution consisting of 0.7 M HCl and 20 mM dicyandiamide (20 segments).

Preparation of Water Samples. Water samples were submitted to an initial filtration process through a 0.25 μm poly(tetrafluoroethylene) (PTFE) membrane filter. Then, they were injected into a 0.1 M PB solution for subsequent electrochemical assessments. The quantity of HYZ in the prepared samples was assessed through our proposed methodology coupled with a standard addition method.

RESULTS AND DISCUSSION

Surface Morphology of DCD-SPCE*. SEM images of the SPCE* are depicted in Figure 1A. As can be seen in Figure 1B, the poly DCD-SPCE* surface generated small sponge-like white structures dispersed over the graphite indicating the polymer formation. The DCD-SPCE* surface was also characterized by means of XPS techniques as a confirmation of the presence of the polymeric film. The DCD polymer formation on the SPCE* proceeded through the establishment of an azo-type bond assisted by the in situ electrogenerated chlorine. The XPS characterization was carried out to obtain chemical information on the modified electrode surface. The C 1s spectral analysis revealed the presence of characteristic peaks at 284.2 eV (corresponding to C−C bonds), 285.6 eV (associated with C−OH bonds), 286.3 eV (indicating C−O bonds), and 288.2 eV (attributed to O−C═O bonds). This finding serves as a strong confirmation for the development of oxygen functionalities on the preanodized SPCE electrode surface (Figure 1C). As indicated in Figure 1D, in the deconvoluted N 1s spectra of DCD-SPCE*, distinct peaks are observed at approximately 398.5, 399.6, and 401.4 eV, providing clear signs of imine nitrogen, neutral amine, and carbon−nitrogen−hydrogen (C−N−H) functional groups. Furthermore, the appearance of a peak at nearly 400.2 eV is indicative of the azo-functional group. As the DCD compound does not possess any azo-functional group, it confirms the polymerization through the generation of an azo-bond. The AFM imaging in Figure 1E offers visual confirmation of the surface modification observed in the DCD-SPCE*. The DCD-modified SPCE* exhibits a disorganized morphology with an approximate size of 2.5 μm corresponding to the DCD polymer. The crumpled upper area is primarily a consequence of the increased growth and strong adhesion of the thin film.

Electrochemical Polymerization and Hydrazine Detection. *DCD Polymerization.* To start with, the polymerization of DCD on the SPCE* was carried out in a 0.7 M HCl supporting electrolyte through repeatedly cycling the potential in the range +0.2 to +1.55 V (versus Ag/AgCl) (Figure 2). In this cyclic voltammogram, at around 1.1 V, an oxidation peak emerged, denoting the transformation of dissolved chloride ions into chlorine.[36,37] At roughly 0.8 V, a reduction peak was detected that can be ascribed to the reduction of chlorine produced electrochemically. Apart from these, a couple of redox peaks were observed at ∼0.50 and ∼0.64 V that were

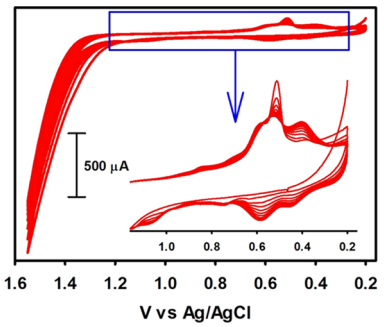

Figure 2. Cyclic voltammogram of DCD polymerization in 0.7 M HCl at pH 1.0.

associated with the polymerized DCD compound. To confirm this, the SPCE* underwent scanning over the range −0.2 to +0.8 V in a 0.1 M PB solution in the absence of DCD and there were no characteristic results that could be observed to prove the existence of immobilized molecules on the electrode. Since the presence of reversible peaks associated with polymerized DCD, from ∼0.50 to ∼0.64 V, can only be observed in the presence of the HCl supporting electrolyte with pH 1.0 (≤), chloride-containing supporting electrolytes are of essence. Various Cl^--enriched supporting electrolytes like NaCl, KCl, $MgCl_2$, and $CaCl_2$ were utilized upon the polymerization processes. However, no redox peaks were observed under any of these environments similar to our earlier report.[38] Based on the above observation, a potential influence of protonation, which may be essential for the DCD oxidation process, is assumed. Finally, the redox peaks of the oxidized form of the DCD compound could be observed only at pH 1.0 (≤), and the oxidation carried out with different parameters failed to elicit redox response upon repetition. A previous investigation has established that the presence of an acidic pH is essential for stabilizing the radical cation, facilitating the synthesis of the polymer. Thus, a similar mechanism of polymelamine and polyaniline can be attributed in the case of DCD as well.[39,40] In addition, we examined the effect of varied concentration of the HCl electrolyte, ranging between 0.1 and 1.0 M, and observed 0.7 M HCl exhibiting a higher response for hydrazine oxidation.

As previously reported, the electrochemically produced Cl_2 undergoes dissolution in an aqueous medium resulting in $Cl_2(aq)/Cl_3^-$/HOCl in an aqueous medium.[41] The electrochemically produced Cl_2 can affect the chemical oxidation of the amine performance in DCD to produce chloramine.[42,43] Further, the electro-reduction of chloramine at ∼0.8 V can lead to the formation of a nitrogen-centered radical,[44] and in turn, this nitrogen-centered radical can react with oxygen functional groups at the SPCE* via the covalent bond.[37,45] However, the DCD also has an additional free amine group ($-NH_2$), which can also follow the above-mentioned mechanism to form another nitrogen-centered radical with the help of electrogenerated chlorine. We thus propose that the nitrogen-centered radical can combine with another nitrogen-centered radical of DCD to form a polymer containing −NH−NH− (hydrazo). This assumption is also supported by the above XPS results.

Electrochemical Behavior of Hydrazine. As shown in Figure 3, because of the lack of hydrazine, no specific response was detected at SPCE* (curve A) and DCD-SPCE* (curve C). Figure 3 (curve B) shows the cyclic voltammetric performance

https://doi.org/10.1021/acs.iecr.3c02669
Ind. Eng. Chem. Res. 2023, 62, 18271−18279

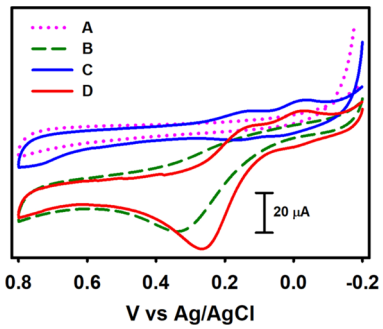

Figure 3. Cyclic voltammetric behavior without and with 1 mM HYZ on SPCE* (A, B) and DCD-SPCE* (C, D).

of hydrazine at SPCE* in 0.1 M PB. The electrochemical detection of hydrazine at SPCE* requires a slightly excess overpotential (~0.4 V) and resulted in a lower current response (curve B). However, the detection of hydrazine at DCD-modified SPCE* exhibited an increased current response with a lower overpotential of ~0.3 V (curve D). As observed, hydrazine is easily involved in the hydrogen-bonding formation (NH···N), onto the DCD-SPCE* surface,[46−47484950] and consequently then triggering the onset potential for sensitive detection of hydrazine through the ECE mechanism.[51−53]

Figure 4A shows the amperometric curves at DCD-SPCE* without (curve a) and with various concentrations (curves b−g), from 100 to 1000 μM, of HYZ. The amperometric curve revealed an orderly increase in anodic current with the HYZ concentration, and a linear relationship was found among the current tested at 25 s with all of the HYZ concentrations (inset of Figure 4 A). Additionally, the diffusion coefficient of hydrazine at DCD-SPCE* in 0.1 M PB was calculated using the Cottrell equation, eq 1.

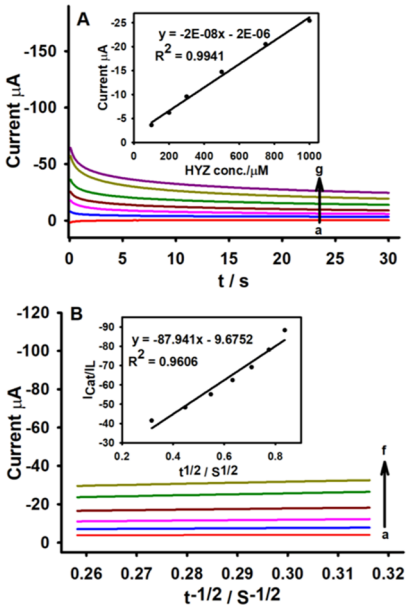

Figure 4. (A) Amperometric response of HYZ: (a) 0 μM, (b) 100 μM, (c) 200 μM, (d) 300 μM, (e) 500 μM, (f) 750 μM, and (g) 1000 μM in 0.1 M PB. Inset: current response at 25 s versus numerous HYZ dilutions. (B) Plots of current response versus $t^{-1/2}$ at numerous HYZ dilutions. Inset suggests the graph of I_{cat}/I_L vs $t^{1/2}$ at 1 mM of HYZ.

$$I = n\pi^{-1/2}t^{-1/2}D^{1/2}\mathrm{FAC} \quad (1)$$

Based on amperometry data at intermediate times, a graph of HYZ current vs $Qt^{-1/2}$ is drawn for numerous HYZ dilutions (Figure 4B) and the average diffusion coefficient value is estimated to be 6.5×10^{-6} cm^2 s^{-1}.

The catalytic reaction rate constant (k) is estimated by eq 2:

$$I_{cat}/I_L = (\pi kCt)^{1/2} \quad (2)$$

The slope of the plot I_{cat}/I_L vs $t^{1/2}$ with 1 mM HYZ (inset of Figure 4B) and the calculated "k" was 246069.71 M^{-1} S^{-1}.

Figure 5 shows the performance of the scan rate at peak current of 1.0 mM HYZ in the range 10−200 mV s^{-1} in 0.1 M PB. The peak currents (ip_a) go up linearly with the increasing scan rate. The logarithmic plot of the HYZ oxidation peak response against the scan rate (Figure 5, Inset) yielded a slope of ~0.37, indicating a diffusion control behavior,[51] and the linear regression (eq 3) shown as follows:

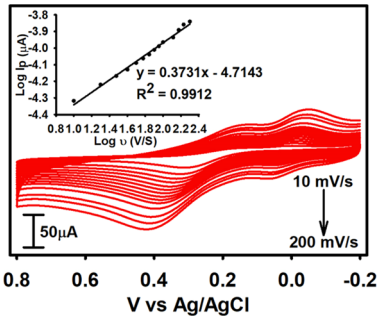

Figure 5. Cyclic voltammograms recorded for DCD-SPCE* at various scan rates, with the solution containing 1.0 mM HYZ in 0.1 M PB at pH 7.4 (a−i: 10, 20, 30, 40, 50, 60, 70, 80, 90, 100, 120, and 150 mV s^{-1}). Inset graph showing the logarithmic plot of scan rate versus peak current.

$$\text{peak: } Ep_a = 0.3731x - 4.7143 (R^2 = 0.9912) \quad (3)$$

Figure 6A illustrates the pH analysis of DCD-SPCE* at various pH values between 5.0 and 9.0, with 1 mM HYZ in 0.1 M PB. Observing the data, it becomes evident that as the pH values increase, the oxidation peak potential of HYZ (E_p) shifts to a negative side. The graph depicting the relationship between E_p and pH reveals a linear connection, characterized by a slope of 58 mV/pH as illustrated in Figure 6 B. The system demonstrated Nernstian behavior with the observed slope value closely approximating the predicted value of 59 mV/pH. This alignment suggests an equilibrium between the number of electrons and protons engaged in the reaction. The activity aligns with findings in previous studies,[60] which mentioned the reaction given below for the hydrazine detection:

$$-N = N - + N_2H_4 \rightarrow -HN - NH - + N_2 + 4H^+ + 4e^- \quad (4)$$

The confirmation of accelerating electron transfer of DCD modified on the SPCE and the difference in electrochemical responses of the DCD-SPCE*, SPCE*, and unmodified SPCE were monitored using CV in 5 mM $[Fe(CN)_6]^{3-/4-}$ solution in a 0.1 M KCl electrolyte (Figure 7A). The standard reversible behavior of the Fe^{II}/Fe^{III} redox pair was detected for the DCD-SPCE*, SPCE*, and unmodified SPCE. Importantly, the

https://doi.org/10.1021/acs.iecr.3c02669
Ind. Eng. Chem. Res. 2023, 62, 18271−18279

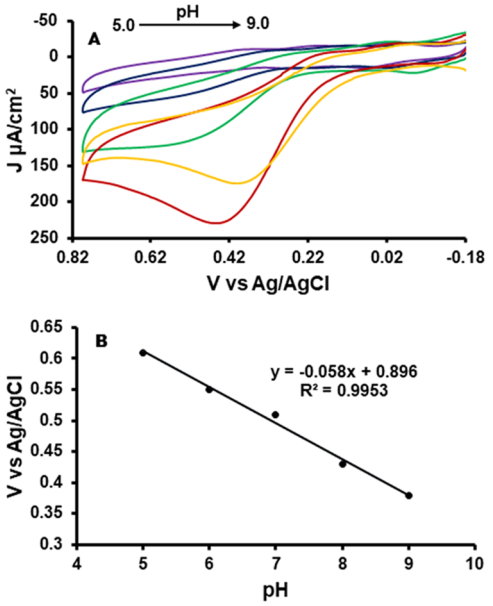

Figure 6. (A) Cyclic voltammograms of DCD-SPCE* at multiple pH in 0.1 M PB (pH 5−9). (B) Plot of pH vs potential.

DCD-SPCE* has the highest redox peak current signal, and SPCE has very low redox peak current signal. Furthermore, a meaningful reduction in the peak-to-peak potential difference (ΔE_p) values between 125 and 80 mV was noticed in SPCE against DCD-SPCE*, correspondingly. This proves that modified DCD-SPCE* is highly electroconductive, stimulates electron transfer, and enhances the active electrode surface area. Electrochemical impedance spectroscopy (EIS) is a reliable practice to check electron-transfer kinetics between heterogeneous interfaces. The electron-transfer process and the active surface area of DCD-SPCE* were additionally estimated using EIS outcomes for the 5 mM $[Fe(CN)_6]^{3-/4-}$ solution in a 0.1 M KCl electrolyte[38] with a Randles equivalent circuit (Figure 7B inset). The Nyquist plot includes two parts: a semicircular segment at higher frequencies that agrees with the charge-transfer resistance (R_{ct}) that influences the electron-transfer step, and a linear segment in a lower frequency range that agrees with the diffusion process. A large half-circle was obtained for unmodified SPCE (548 kΩ), which exhibited considerable electron-transfer hindrance (Figure 7B). The R_{ct} values were found to be 1.02×10^{-4} and 2.98×10^{-4} kΩ for the SPCE*-DCD and SPCE*, respectively. The DCD-SPCE* was observed with the smallest R_{ct} value (1.02×10^{-4} kΩ) when compared with other electrodes. This result suggests that the modification of the SPCE* with DCD could be qualified to the augmentation of both active surface area and conductivity.

Analytical Performance. To further test the analytical utility, a DCD-SPCE* was coupled with a wall-jet electrochemical flow injection analysis (FIA) system to detect and quantify hydrazine. The optimum working potential and the flow rate for hydrazine detection at FIA with 1 mM HYZ were analyzed at various potentials and flow rates at 0.1 M PB in the mobile phase. Finally, we decided to use 0.35 V and 0.2 mL min^{-1} for the HYZ detection. Under the optimized condition, the FIA (Figure 8A,C) results indicated a linear response between 20 nM and 70 μM and also from 100 μM to 1 mM of HYZ in 0.1 M PB with R^2 values of 0.9999 and 0.996 (Figure 8B,D) and a detection limit (LOD) of 6.7 nM. The calculated specific sensitivity of the DCD-SPCE* was 0.1 nA nM^{-1} cm^{-2}.[62] Further, a comparison study based on analytical sensitivity of the DCD-SPCE* with other polymer/metal nanostructure-modified carbon electrodes is presented in Table 1. In addition, the duplicability (n = 6) and consistency (n = 10) of the DCD-SPCEs* were studied using CV and FIA experiments. Relative standard deviation (RSD) values of 1.96 and 0.7 for the electrode−electrode reproducibility and repeatability were obtained, respectively (Figure 9). Results obtained under the dynamic amperometric method of flow injection condition also established a better operational permanence of the electrodes. The plausible electro active interfering materials during hydrazine detection have been investigated using FIA technique in 0.1 M PB (pH 7.4).

As shown in Figure 10, addition of 100 μM hydrazine showed a higher current signal, while injections of 150 μM concentration of interferents like oxalic acid, glucose, lactose, fructose, sucrose, L-arginine, L-tryptophan, Na^+, K^+, ammonium ion, CO_3^{2-}, nitrate ion, Cl^-, SO_4^{2-}, and acetate ion did not show any response. The DCD-SPCE* showed a good tolerance to all of these interfering substances.

Real Sample Analysis. To analyze the capability of the modified electrode toward the deduction of HYZ in environmental samples, lake water and tap water samples were studied.

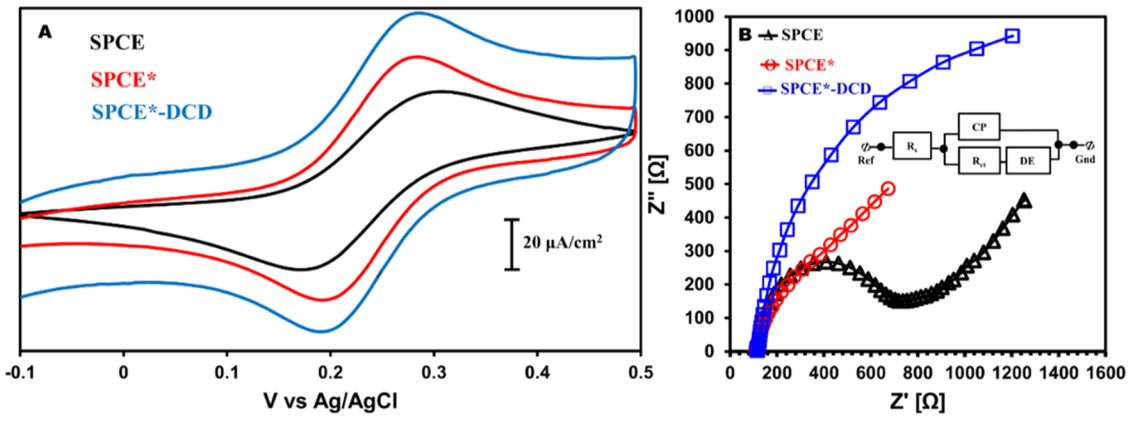

Figure 7. Representative (A) CV of SPCE, SPCE*, & DCD-SPCE* in 5 mM$[Fe(CN)6]^{3-/4-}$ solution in 0.1 M KCl and (B) EIS curves of SPCE, SPCE*, and DCD-SPCE* in 0.1 M KCl solution enriched with 5 mM $[Fe(CN)6]^{3-/4-}$. The inset included within figure (B) presents the circuit model used to fit the EIS data.

https://doi.org/10.1021/acs.iecr.3c02669
Ind. Eng. Chem. Res. 2023, 62, 18271−18279

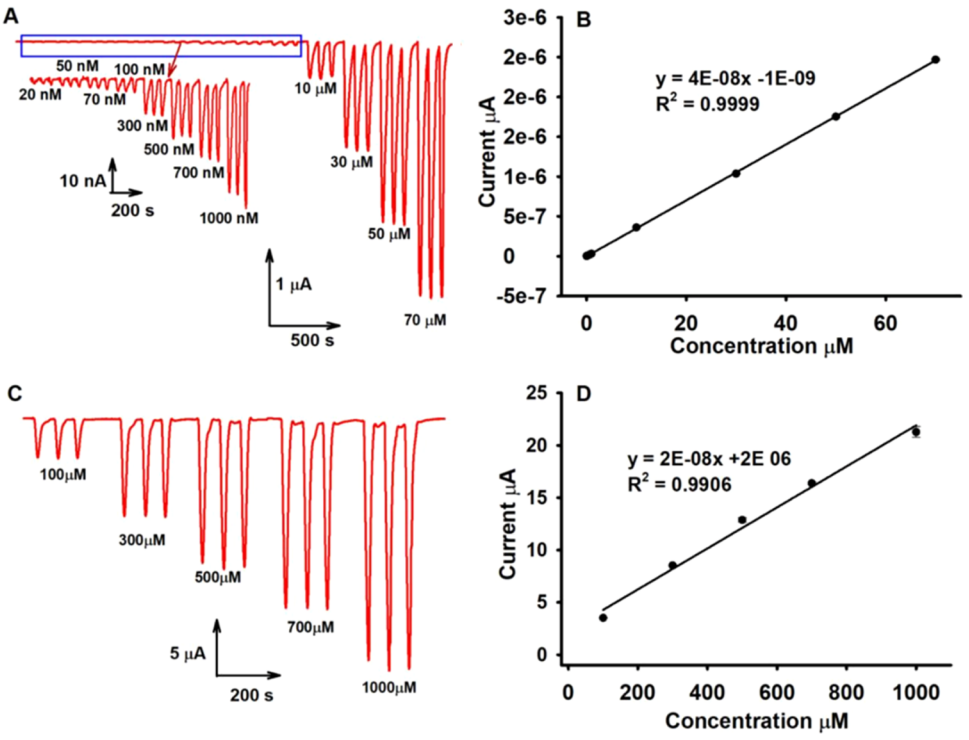

Figure 8. FIA response acquired with increasing strengths of HYZ in 0.1 M PB. Linear response between 20 nM and 70 μM and also from 100 μM to 1 mM (A&C) with R^2 values 0.9999 and 0.9906 (B&D).

Table 1. Comparison Data for the Detection of HYZ with Different HYZ Sensors[a]

s. no	modified electrode	electrochemical method	pH	linear range (μM)	LOD (μM)	references
1	PTh/ZnO/GCE	amperometric	7.4	0.5−48	0.207	54
2	chlorogenic acid/carbon ceramic	amperometric	8.0	0.1−1000	0.02	35
3	HMWCNT/GCE	amperometric	7.0	2.0−122.8	0.68	55
4	*o*-aminophenol/GCE	amperometric	9.0	2.0−20	0.5	56
5	hydroquinone salophen/GCE	cyclic voltammetry	7.5	10−400	1.6	57
6	ErGO/PEDOT:PSS/GCE	amperometric	7.0	0.2−100	0.01	32
7	N-HCSs/SPGE	DPV	7.0	0.02−380	0.007	29
8	PB/CNP/PPy/GC	amperometric		0.75−1653	0.29	58
9	CIT/MCM41/carbon paste	DPV	7.0	0.01−200	0.0033	59
10	AuNPs/CNT/poly(NB)/GCE	amperometric	7.4	1−440	0.33	60
11	AuNPs/CNTs-ErGO/GC	amperometric	7.4	0.3−319	0.065	9
12	ZIF-Ni/ITO	amperometric		2.5−28,000	0.021	33
13	Au-MSM/GC	amperometric	7.0	5−18,000	0.11	7
14	Pt/HNPG	amperometric	7.0	5−6105	1.03	61
15	Pcv/PGE	FIA	9.0	0.25−500	0.08	19
16	DCD-SPCE*	FIA	7.4	0.02−1000	0.0067	this work

[a] GCE, glassy carbon; PTh, polythiophene; HMWCNT, hematoxylin multiwall carbon nanotube; ErGO, electrochemically reduced graphene oxide; PEDOT, poly(3,4-ethylenedioxythiophene); PSS, poly(styrene sulfonate); N-HCSs, nitrogen-doped hollow carbon spheres; SPGE, screen-printed graphite electrode; DPV, differential pulse voltammetry; PB, Prussian blue; CNP/PPy, carbon nanopolyhedra/polypyrrole; CIT, 5-(5-chloro-2,4-dihydroxyphenyl)imidazo[4,5-*d*] [1,3]thiazin-7(3*H*)-one; MCM-41, mesoporous material based on silica; AuNPs, gold nanoparticles; poly(NB), poly(Nile blue); CNT, carbon nanotube; ZIF-Ni, zeolitic imidazolate framework 8 (ZIF-8) and porous nickel films; Au, gold nanoparticles; MSM, mesoporous silica microspheres; Pt, platinum nanoparticles; HNPG, highly surface-roughened nanoporous gold electrode; PGE, pencil graphite electrode; Pcv, pyrocatechol violet.

Because significant HYZ was unable to be detected in the water samples, quantifiable amounts of HYZ were mixed in different water samples and a standard addition method was further adopted to ascertain the recovery values. The data are presented in Table 2. The recovery values fall between 97.2 and 103.7% with a maximum RSD of 3.88 (n = 3). The calculated recovery and RSD validate that the suggested method is appropriate for efficient hydrazine detection in tap and lake water.

CONCLUSIONS

The DCD-SPCE* has been demonstrated as a facile technique for the electrochemical detection of HYZ under decreasing overpotential (~0.3 V vs Ag/AgCl) in neutral medium (0.1 M, pH 7.4 PB). The presence of an azo moiety assisted the

https://doi.org/10.1021/acs.iecr.3c02669
Ind. Eng. Chem. Res. 2023, 62, 18271−18279

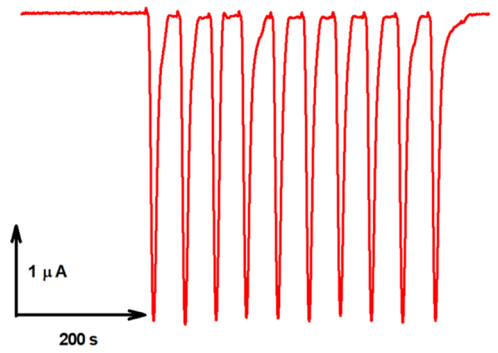

Figure 9. FIA response was derived from a sequence of ten injections, each consisting of 100 μM HYZ into a 0.1 M PB.

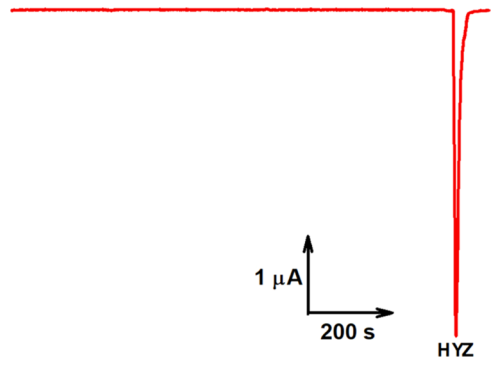

Figure 10. FIA response for injection of 150 μM of interferents along with 100 μM HYZ in 0.1 M PB, pH 7.4.

Table 2. Real Sample Analysis Data of HYZ

samples	added (nM)	detected (nM)	recovery (%)	RSD (%)
tap water	50.0	51.10	101.1	3.53
	100.0	98.70	98.7	3.88
	500.0	498.20	98.2	3.30
	1000.00	1000.50	100.5	0.58
	10000.00	10002.80	102.8	0.42
lake water	50.0	53.70	103.7	3.27
	100.0	100.80	100.8	2.38
	500.0	498.40	98.4	3.77
	1000.00	997.20	97.2	1.24
	10000.00	9997.90	97.9	0.82

electrocatalytic oxidation of HYZ to lower the overpotential, and the existence of other nitrogen functionalities facilitated the hydrogen bonding between the electrode surface and the analyte to improve the sensitivity. The modified DCD-SPCE* exhibited excellent analytical utility and good recoveries for the hydrazine detection in the environmental water samples, making it highly suitable for the detection of hydrazine in environmental water from the tap and lake.

AUTHOR INFORMATION

Corresponding Author

Gopinathan Manavalan − *Department of Chemistry, National Chung Hsing University, 402 Taichung, Taiwan; Wallenberg Wood Science Center, Technical Chemistry, Department of Chemistry, Chemical-Biological Centre, Umeå University, SE-901 87 Umeå, Sweden; Department of Forest Biomaterials and Technology, Swedish University of Agricultural Sciences (SLU), SE-90183 Umeå, Sweden;* orcid.org/0000-0001-6533-3576; Phone: +46(0)76-9672299; Email: gopinathan.manavalan@umu.se

Authors

Thiyagarajan Natarajan − *Department of Chemistry, National Chung Hsing University, 402 Taichung, Taiwan*

Kayode Omotayo Adeniyi − *Department of Chemistry, Chemical-Biological Centre, Umeå University, SE-901 87 Umeå, Sweden;* orcid.org/0000-0002-6196-5805

Jyh-Myng Zen − *Department of Chemistry, National Chung Hsing University, 402 Taichung, Taiwan*

Solomon Tesfalidet − *Department of Chemistry, Chemical-Biological Centre, Umeå University, SE-901 87 Umeå, Sweden;* orcid.org/0000-0002-8175-6883

Mikael Thyrel − *Department of Forest Biomaterials and Technology, Swedish University of Agricultural Sciences (SLU), SE-90183 Umeå, Sweden*

Torbjörn A. Lestander − *Department of Forest Biomaterials and Technology, Swedish University of Agricultural Sciences (SLU), SE-90183 Umeå, Sweden*

Subba Reddy Alla − *Analytical Development Laboratory, Apicore LLC, Somerset, New Jersey 08873, United States;* orcid.org/0000-0002-6291-5420

Jyri-Pekka Mikkola − *Wallenberg Wood Science Center, Technical Chemistry, Department of Chemistry, Chemical-Biological Centre, Umeå University, SE-901 87 Umeå, Sweden; Laboratory of Industrial Chemistry and Reaction Engineering, Johan Gadolin Process Chemistry Centre, Åbo Akademi University, FI-20500 Turku, Finland*

Complete contact information is available at: https://pubs.acs.org/10.1021/acs.iecr.3c02669

Notes

The authors declare no competing financial interest.

ACKNOWLEDGMENTS

The authors thankfully acknowledge the funding provided by the Bio4Energy programme, Kempe Foundations [JCK-JCK-2140 and JCSMK23-0075], Wallenberg Wood Science Center under auspices of Alice and Knut Wallenberg Foundation, and the Ministry of Science and Technology, Taiwan. The authors conducted experiments at the Technical Chemistry, Department of Chemistry, Chemical-Biological Centre, Umeå University, Sweden, and also at the Johan Gadolin Process Chemistry Centre at Åbo Akademi University in Finland. In this work, the authors particularly wish to honor the late Carl Kempe of Kempe Foundations who for so many years has supported them: rest in peace. They also acknowledge Dr. Shamasree Ghosh and Dr. Tamilselvi Shanmugam for their help with AFM. Additionally, this article represents a considerable portion of Gopinathan Manavalan's doctoral research conducted at National Chung Hsing University, Taiwan.

REFERENCES

(1) Golabi, S. M.; Zare, H. R. Electrocatalytic oxidation of hydrazine at a chlorogenic acid (CGA) modified glassy carbon electrode. *J. Electroanal. Chem.* **1999**, *465*, 168−176.

(2) Ensafi, A. A.; Mirmomtaz, E. Electrocatalytic oxidation of hydrazine with pyrogallol red as a mediator on glassy carbon electrode. *J. Electroanal. Chem.* **2005**, *583*, 176−183.

(3) Reja, S. I.; Gupta, N.; Bhalla, V.; Kaur, D.; Arora, S.; Kumar, M. A. Charge transfer based ratiometric fluorescent probe for detection

of hydrazine in aqueous medium and living cells. *Sens. Actuators, B* **2016**, *222*, 923−929.
(4) Krittayavathananon, A.; Srimuk, P.; Luanwuthi, S.; Sawangphruk, M. Palladium Nanoparticles Decorated on Reduced Graphene Oxide Rotating Disk Electrodes toward Ultrasensitive Hydrazine Detection: Effects of Particle Size and Hydrodynamic Diffusion. *Anal. Chem.* **2014**, *86*, 12272−12278.
(5) Wang, C.; Zhang, L.; Guo, Z.; Xu, J.; Wang, H.; Zhai, K.; Zhuo, X. A novel hydrazine electrochemical sensor based on the high specific surface area graphene. *Microchim. Acta* **2010**, *169*, 1−6.
(6) Giroud, F.; Gross, A.; Junior, D. F.; Holzinger, M.; De Campos, C. M.; Acuña, J.; Domingos, J.; Cosnier, S. Hydrazine Electrooxidation with PdNPs and Its Application for a Hybrid Self-Powered Sensor and N2H4 Decontamination. *J. Electrochem. Soc.* **2017**, *164*, 3052−3057.
(7) Gupta, R.; Rastogi, P. K.; Ganesan, V.; Yadav, D. K.; Sonkar, P. K. Gold nanoparticles decorated mesoporous silica microspheres: A proficient electrochemical sensing scaffold for hydrazine and nitrobenzene. *Sens. Actuators, B* **2017**, *239*, 970−978.
(8) Rahman, M. M.; Alfonso, V. G.; Fabregat-Santiago, F.; Bisquert, J.; Asiri, A. M.; Alshehri, A. A.; Albar, H. A. Hydrazine sensors development based on a glassy carbon electrode modified with a nanostructured TiO2 films by electrochemical approach. *Microchim. Acta* **2017**, *184*, 2123−2129.
(9) Zhao, Z.; Sun, Y.; Li, P.; Zhang, W.; Lian, K.; Hu, J.; Chen, Y. Preparation and characterization of AuNPs/CNTs-ErGO electrochemical sensors for highly sensitive detection of hydrazine. *Talanta* **2016**, *158*, 283−291.
(10) Kannan, P. K.; Moshkalev, S. A.; Rout, C. S. Electrochemical sensing of hydrazine using multilayer graphene nanobelts. *RSC Adv.* **2016**, *6*, 11329−11334.
(11) Chen, R.; Hu, T.; Xing, S.; Wei, T.; Chen, J.; Li, T.; Niu, Q.; Zhang, Z.; Ren, H.; Qin, X. A dual-responsive fluorescent turn-on sensor for sensitively detecting and bioimaging of hydrazine and hypochlorite in biofluids, live-cells, and plants. *Anal. Chim. Acta* **2023**, *1239*, No. 340735.
(12) Subramanian, S.; Narayanasastri, S.; Reddy, A. R. K. Doping-induced detection and determination of propellant grade hydrazines by a kinetic spectrophotometric method based on nano and conventional polyaniline using halide ion releasing additives. *RSC Adv.* **2014**, *4*, 27404−27413.
(13) Timchenko, Y. V.; Apenkina, A.; Smolenkov, A.; Pirogov, A.; Shpigun, O. Simultaneous determination of hydrazine, methylhydrazine and 1, 1-dimethylhydrazine in waters by HPLC with spectrophotometric detection using catalysis to obtain derivatives. *J. Anal. Chem.* **2021**, *76*, 1163−1171.
(14) Oh, J. A.; Shin, H. S. Simple determination of hydrazine in waste water by headspace solid-phase micro extraction and gas chromatography-tandem mass spectrometry after derivatization with trifluoro pentanedione. *Anal. Chim. Acta* **2017**, *950*, 57−63.
(15) Safavi, A.; Baezzat, M. Flow injection chemiluminescence determination of hydrazine. *Anal. Chim. Acta* **1998**, *358*, 121−125.
(16) Xu, G.; Guo, N.; Zhang, Q.; Wang, T.; Song, P.; Xia, L. An ultrasensitive surface-enhanced Raman scattering sensor for the detection of hydrazine via the Schiff base reaction. *J. Hazard Mater.* **2022**, *424*, No. 127303.
(17) Liu, Y.; Chen, S. S.; Wang, A. J.; Feng, J. J.; Wu, X.; Weng, X. An ultra-sensitive electrochemical sensor for hydrazine based on AuPd nanorod alloy nanochains. *Electrochim. Acta* **2016**, *195*, 68−76.
(18) Gao, F.; Wang, Q.; Gao, N.; Yang, Y.; Cai, F.; Yamane, M.; Gao, F.; Tanaka, H. Hydroxyapatite/chemically reduced graphene oxide composite: Environment-friendly synthesis and high-performance electrochemical sensing for hydrazine. *Biosens. Bioelectron.* **2017**, *97*, 238−245.
(19) Ayaz, S.; Dilgin, Y. Flow injection amperometric determination of hydrazine based on its electrocatalytic oxidation at pyrocatechol violet modified pencil graphite electrode. *Electrochim. Acta* **2017**, *258*, 1086−1095.
(20) Yang, C. C.; Kumar, A. S.; Kuo, M. C.; Chien, S. H.; Zen, J. M. Copper−palladium alloy nanoparticle plated electrodes for the electrocatalytic determination of hydrazine. *Anal. Chim. Acta* **2005**, *554*, 66−73.
(21) Šljukić, B.; Banks, C. E.; Crossley, A.; Compton, R. G. Iron (III) oxide graphite composite electrodes: application to the electroanalytical detection of hydrazine and hydrogen peroxide. *Electroanalysis* **2006**, *18*, 1757−1762.
(22) Kumar, A. S.; Gandhi, M.; Saikrithika, S.; Dinesh, B.; Shafeeq, S.; Ganesh, V. Localized formation of highly surface-active gold nanoparticle on intrinsic Nickel containing carbon black and its scanning electrochemical microscopy interrogation and electrocatalytic oxidation of hydrazine. *Electrochim. Acta* **2023**, *443*, No. 141937.
(23) Zhang, Y.; Wu, J.; Zhao, S.; Tang, X.; He, Z.; Huang, K.; Yu, H.; Zou, Z.; Xiong, X. Self-assembled ZnO microspheres coated with carbon dot-doped CoNi LDH wrinkled films as electrochemical sensors for highly sensitive detection of hydrazine. *Anal. Methods* **2023**, *15*, 304−310.
(24) Sanatkar, T. H.; Khorshidi, A.; Sohouli, E.; Janczak, J. Synthesis, crystal structure, and characterization of two Cu (II) and Ni (II) complexes of a tetradentate N_2O_2 Schiff base ligand and their application in fabrication of a hydrazine electrochemical sensor. *Inorg. Chim. Acta.* **2020**, *506*, No. 119537.
(25) Ayaz, S.; Dilgin, Y.; Apak, R. Flow injection amperometric determination of hydrazine at a cupric-neocuproine complex/anionic surfactant modified disposable electrode. *Microchem. J.* **2020**, *159*, No. 105457.
(26) Wang, J.; Chicharro, M.; Rivas, G.; Cai, X.; Dontha, N.; Farias, P. A.; Shiraishi, H. DNA biosensor for the detection of hydrazines. *Anal. Chem.* **1996**, *68*, 2251−2254.
(27) Yan, L.; Bo, X.; Zhang, Y.; Guo, L. Facile green synthesis of nitrogen-doped porous carbon and its use for electrocatalysis towards nitrobenzene and hydrazine. *Electrochim. Acta* **2014**, *137*, 693−699.
(28) Jilani, F.; Husnain, M.; Nawaz, F.; Mohsin, M. A.; Iqbal, N.; Iqbal, J.; Abd El-Fattah, A. A Facile Synthesis of WO_3/g-C_3N_4 Composite for Chemical Sensing of Dopamine and Hydrazine. *Mater. Lett.* **2023**, *343*, No. 134391.
(29) Tajik, S.; Sharifi, F.; Beitollahi, H. Differential Pulse Voltammetric Analysis of Hydrazine in Water Samples by Using Screen-Printed Graphite Electrode Modified with Nitrogen-Doped Hollow Carbon Spheres. *Ind. Eng. Chem. Res.* **2023**, *62*, 4694−4703.
(30) Gowthaman, N.; Mohapatra, D.; Arul, P.; Chang, W. S. Ultrasonic-assisted decoration of AuNPs on carbon nano-onions as robust electrochemical scaffold for sensing of carcinogenic hydrazine in industrial effluents. *J. Ind. Eng. Chem.* **2023**, *117*, 227−237.
(31) Saengsookwaow, C.; Rangkupan, R.; Chailapakul, O.; Rodthongkum, N. Nitrogen-doped graphene−poly-(vinylpyrrolidone)/gold nanoparticles modified electrode as a novel hydrazine sensor. *Sens. Actuators, B* **2016**, *227*, 524−532.
(32) Rahman, H. A.; Rafi, M.; Putra, B. R.; Wahyuni, W. T. Electrochemical Sensors Based on a Composite of Electrochemically Reduced Graphene Oxide and PEDOT: PSS for Hydrazine Detection. *ACS Omega* **2023**, *8*, 3258−3269.
(33) Shi, E.; Lin, H.; Wang, Q.; Zhang, F.; Shi, S.; Zhang, T.; Li, X.; Niu, H.; Qu, F. Synergistic effect of the composite films formed by zeolitic imidazolate framework 8 (ZIF-8) and porous nickel films for enhanced amperometric sensing of hydrazine. *Dalton Trans.* **2017**, *46*, 554−563.
(34) Shahid, M. M.; Rameshkumar, P.; Basirunc, W. J.; Wijayantha, U.; Chiu, W. S.; Khiew, P. S.; Huang, N. M. An electrochemical sensing platform of cobalt oxide@ gold nanocubes interleaved reduced graphene oxide for the selective determination of hydrazine. *Electrochim. Acta* **2018**, *259*, 606−616.
(35) Salimi, A.; Hallaj, R. Adsorption and reactivity of chlorogenic acid at a hydrophobic carbon ceramic composite electrode: application for the amperometric detection of hydrazine. *Electroanalysis* **2004**, *16*, 1964−1971.

https://doi.org/10.1021/acs.iecr.3c02669
Ind. Eng. Chem. Res. 2023, 62, 18271−18279

(36) Kim, E. Y.; Kim, M. S.; Lee, J. C.; Yoo, K.; Jeong, J. Leaching behavior of copper using electro-generated chlorine in hydrochloric acid solution. *Hydrometallurgy* **2010**, *100*, 95−102.
(37) Senthilkumar, K.; Sithini, T. N.; Thiyagarajan, N.; Baskar, S.; Zen, J. M. Facile and stable immobilization of adenine on screen printed carbon electrode assisted by electrogenerated chlorine for electrocatalytic oxidation of NADH. *Electrochem. Commun.* **2015**, *60*, 113−116.
(38) Natarajan, T.; Gopinathan, M.; Thiruppathi, M.; Adeniyi, O.; Chang, J. L.; Zen, J. M.; Tesfalidet, S.; Mikkola, J. P. Detection of nitrification inhibitor Dicyandiamide: A direct electrochemical approach. *Food Chem.: X* **2023**, *18*, No. 100658.
(39) Baskar, S.; Liao, C. W.; Chang, J. L.; Zen, J. M. Electrochemical synthesis of electroactive poly(melamine) with mechanistic explanation and its applicability to functionalize carbon surface to prepare nanotube−nanoparticles hybrid. *Electrochim. Acta* **2013**, *88*, 1−5.
(40) Mu, S.; Kan, J. Evidence for the autocatalytic polymerization of aniline. *Electrochim. Acta* **1996**, *41*, 1593−1599.
(41) Gray, K. M.; Liba, B. D.; Wang, Y.; Cheng, Y.; Rubloff, G. W.; Bentley, W. E.; Montembault, A.; Royaud, I.; David, L.; Payne, G. F. Electrodeposition of a biopolymeric hydrogel: potential for one-step protein electroaddressing. *Biomacromolecules* **2012**, *13*, 1181−1189.
(42) Hawkins, C. L.; Davies, M. J. Hypochlorite-induced damage to nucleosides: formation of chloramines and nitrogen-centered radicals. *Chem. Res. Toxicol.* **2001**, *14*, 1071−1081.
(43) Qiang, Z.; Adams, C. D. Determination of monochloramine formation rate constants with stopped-flow spectrophotometry. *Environ. Sci. Technol.* **2004**, *38*, 1435−1444.
(44) Piela, B.; Wrona, P. K. Electrochemical behavior of chloramines on the rotating platinum and gold electrodes. *J. Electrochem. Soc.* **2003**, *150*, E255−E265.
(45) Moad, G.; Solomon, D. H. *The Chemistry of Radical Polymerization*; Elsevier Science, 2006.
(46) Lehn, J. M.; Mascal, M.; Decian, A.; Fischer, J. Molecular recognition directed self-assembly of ordered supramolecular strands by cocrystallization of complementary molecular components. *J. Chem. Soc., Chem. Commun.* **1990**, 479−481, DOI: 10.1039/c39900000479.
(47) Whitesides, G. M.; Simanek, E. E.; Mathias, J. P.; Seto, C. T.; Chin, D.; Mammen, M.; Gordon, D. M. Noncovalent synthesis: using physical-organic chemistry to make aggregates. *Acc. Chem. Res.* **1995**, *28*, 37−44.
(48) Sherrington, D. C.; Taskinen, K. A. Self-assembly in synthetic macromolecular systems via multiple hydrogen bonding interactions. *Chem. Soc. Rev.* **2001**, *30*, 83−93.
(49) Ai, K.; Liu, Y.; Lu, L. Hydrogen-bonding recognition-induced color change of gold nanoparticles for visual detection of melamine in raw milk and infant formula. *J. Am. Chem. Soc.* **2009**, *131*, 9496−9497.
(50) Zhao, Z.; Zhang, G.; Gao, Y.; Yang, X.; Li, Y. A novel detection technique of hydrazine hydrate: modality change of hydrogen bonding-induced rapid and ultrasensitive colorimetric assay. *Chem. Commun.* **2011**, *47*, 12816−12818.
(51) Senthilkumar, K.; Zen, J. M. Free chlorine detection based on EC'mechanism at an electroactive polymelamine-modified electrode. *Electrochem. Commun.* **2014**, *46*, 87−90.
(52) Wong, C. S.; Chen, Y. D.; Chang, J. L.; Zen, J. M. Biomolecule-free, selective detection of clenbuterol based on disposable screen-printed carbon electrode. *Electrochem. Commun.* **2015**, *60*, 163−167.
(53) Thiruppathi, M.; Thiyagarajan, N.; Gopinathan, M.; Chang, J. L.; Zen, J. M. A dually functional 4-aminophenylboronic acid dimer for voltammetric detection of hypochlorite, glucose and fructose. *Microchim. Acta* **2017**, *184*, 4073−4080.
(54) Faisal, M.; Harraz, F. A.; Al-Salami, A.; Al-Sayari, S.; Al-Hajry, A.; Al-Assiri, M. Polythiophene/ZnO nanocomposite-modified glassy carbon electrode as efficient electrochemical hydrazine sensor. *Mater. Chem. Phys.* **2018**, *214*, 126−134.
(55) Zare, H. R.; Nasirizadeh, N. Hematoxylin multi-wall carbon nanotubes modified glassy carbon electrode for electrocatalytic oxidation of hydrazine. *Electrochim. Acta* **2007**, *52*, 4153−4160.
(56) Nassef, H. M.; Radi, A. E.; O'Sullivan, C. K. Electrocatalytic oxidation of hydrazine at o-aminophenol grafted modified glassy carbon electrode: Reusable hydrazine amperometric sensor. *J. Electroanal. Chem.* **2006**, *592*, 139−146.
(57) Revenga-Parra, M.; Lorenzo, E.; Pariente, F. Synthesis and electrocatalytic activity towards oxidation of hydrazine of a new family of hydroquinone salophen derivatives: application to the construction of hydrazine sensors. *Sens. Actuators, B* **2005**, *107*, 678−687.
(58) Zhao, J.; Yue, P.; Tricard, S.; Pang, T.; Yang, Y.; Fang, J. Prussian blue (PB)/carbon nanopolyhedra/polypyrrole composite as electrode: a high performance sensor to detect hydrazine with long linear range. *Sens. Actuators, B* **2017**, *251*, 706−712.
(59) Benvidi, A.; Nikmanesh, M.; Tezerjani, M. D.; Jahanbani, S.; Abdollahi, M.; Akbari, A.; Rezaeipoor-Anari, A. A comparative study of various electrochemical sensors for hydrazine detection based on imidazole derivative and different nano-materials of MCM-41, RGO and MWCNTs: Using net analyte signal (NAS) for simultaneous determination of hydrazine and phenol. *J. Electroanal. Chem.* **2017**, *787*, 145−157.
(60) Hatip, M.; Koçak, S.; Dursun, Z. Simultaneous electrochemical determination of hydrazine and nitrite based on Au nanoparticles decorated on the poly (Nile Blue) modified carbon nanotube. *Electroanalysis* **2023**, *35*, No. e202200132.
(61) Pei, Y.; Hu, M.; Xia, Y.; Huang, W.; Li, Z.; Chen, S. Electrochemical preparation of Pt nanoparticles modified nanoporous gold electrode with highly rough surface for efficient determination of hydrazine. *Sens. Actuators, B* **2020**, *304*, No. 127416.
(62) Gopinathan, M.; Thiyagarajan, N.; Thiruppathi, M.; Zen, J. M. Electrocatalytic Oxidation and Flow Injection Analysis of Isoniazid Drug Using an Unmodified Screen Printed Carbon Electrode in Neutral pH. *Electroanalysis* **2018**, *30*, 1400−1406.

https://doi.org/10.1021/acs.iecr.3c02669
Ind. Eng. Chem. Res. 2023, 62, 18271−18279